Extended defects in diamond: The interstitial platelet

J. P. Goss, B. J. Coomer, R. Jones, and C. J. Fall
School of Physics, The University of Exeter, Exeter EX4 4QL, United Kingdom

P. R. Briddon
Department of Physics, The University of Newcastle upon Tyne, Newcastle upon Tyne NE1 7RU, United Kingdom

S. Öberg
Department of Mathematics, Luleå University of Technology, Luleå S-97187, Sweden

(Received 21 June 2002; revised manuscript received 20 November 2002; published 24 April 2003)

The structure and properties of the {001} planar platelet in diamond are investigated using *ab initio* theory. We find that a carbonaceous model, based on a layer of self-interstitials, satisfies the requirements of transmission electron microscopy, infrared absorption data, and energetic considerations. The energetics of self-interstitial production during nitrogen aggregation are considered. It is found that the growth mechanism of the platelet involves a thermally activated release of vacancies from platelets. The role of vacant sites and platelet nitrogen are also investigated and it is shown that these defects embedded within the platelet could account for the observed optical activity.

DOI: 10.1103/PhysRevB.67.165208 PACS number(s): 61.72.Ji, 61.72.Bb, 71.20.Mq, 71.23.An

I. INTRODUCTION

Platelets are {001} planar structures found only in type Ia diamonds, i.e., those containing nitrogen predominantly in aggregated forms. Typical platelets possess a length scale of tens of nanometers, but some extend to a few μm.[1,2] They were first observed in x-ray diffraction measurements[3] as anomalous spikes corresponding to $\{00h\}$ reflections e.g., {001}, {002}, {003} *etc*. These reflections are forbidden by the diamond lattice and their origin was a mystery until Frank[4] suggested that they were due to the condensation of impurities onto {001} planes causing a distortion to tetragonal symmetry. He reasoned that the impurity platelet leads to a lattice displacement of about $0.33a_0\langle 001\rangle$ to account for a weak {003} reflection and suggested Si as the cause because of its size and chemical similarity to carbon.

Transmission electron microscopy (TEM) revealed around 10^{19}–10^{20} atoms cm^{-3} in the platelets[5] and for the original assignment to be correct the concentration of Si would have to be comparable with this. However, analysis of the debris formed when diamonds are burned showed that type Ia diamonds did not contain appreciable amounts of Si but instead copious amounts ($\sim$0.2 at. %) of nitrogen.[6] Lang[7] subsequently proposed an elegant and highly influential model for the platelet shown in Fig. 1 involving a pair of N atoms replacing each carbon atom in a {001} plane. Using simple covalent radii for the N and C atoms, the lattice displacement caused by this platelet is estimated to be $\sim 0.3a_0$, in rough agreement with experiment.[4,8–10] Although the Lang model has formed the basis for many subsequent investigations, electron energy loss (EEL) spectroscopic investigations[11–14] have shown that the concentration of nitrogen within the platelet was very much lower than two monolayers required by the Lang model. Consequently, the Lang model cannot be a correct description of the platelet.

A different model of the platelet had been suggested following a detailed infra-red absorption study by Woods.[15] A correlation between the intensities of the x-ray spikes due to platelets and an infra-red absorption band with a maximum between 1358 and 1373 cm^{-1}, labeled B', had already been noted.[16] The absorption patterns of the two common nitrogen aggregates in type Ia diamonds: the *A* defect composed of a pair of neighboring substitutional nitrogen defects,[17] and the *B* defect composed of a lattice vacancy bordered by four N atoms[18,19] were also known. Woods found that for so-called ''regular'' samples which form the majority, the integrated intensity of the B' band was linearly related to the concentration of *B* centers.[15] Moreover, the densities of atoms in the platelet and the density of *B* centers are comparable.[5] This suggests that the formation of the *B* center and platelet are connected and explains why platelets are rarely found in type IaA diamonds, where there are few *B* centers, and often found in type IaB material containing few *A* centers. Woods then suggested that carbon interstitials could be released when *B* centers were formed, and these then condensed onto $\langle 100\rangle$ planes forming platelets.[15] Such a model based on a layer composed of carbon interstitials could explain another problem with the Lang model encountered by previous theoretical modeling.[20] That study found the vibrations of nitrogen and carbon atoms at the core of the platelet, led to fre-

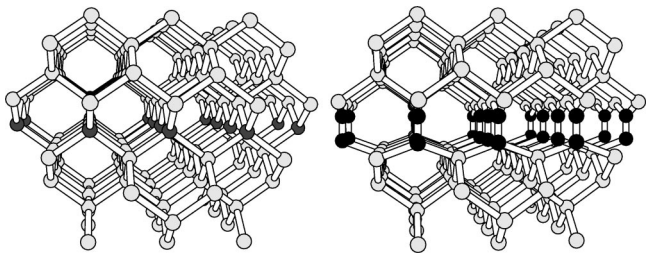

FIG. 1. Schematic of the Lang, nitrogen double layer model for the {001} platelet (Ref. 7). On the left is a section of pure diamond with a {001} layer of C atoms shaded. On the right this plane of atoms has been replaced by pairs of N atoms (shown in black) aligned along $\langle 001\rangle$.

quencies that fell below the Raman frequency and hence the Lang model was unable to account for the B' band.

Annealing studies carried out on type Ib diamonds, where N is in the form of isolated substitutional impurities,[21] revealed that the nitrogen atoms aggregated leading first to the formation of *A* centers and second, at temperatures around 2500 °C, under a stabilizing pressure of around 10 GPa, to *B* centers along with platelets. It is remarkable that a process that took place over millennia in the Earth was reproduced in the laboratory in a few hours. The creation of ''man-made'' platelets then allowed infra-red absorption studies to be undertaken using mixtures of ^{14}N, ^{15}N, ^{12}C, and ^{13}C. These investigations found that the B' band did not appreciably shift with ^{15}N,[22] which rules out a nitrogen origin to the B' band. However, the shift of the peak with ^{13}C was smaller than expected for a purely carbon model. It is possible that this is due to variations in platelet size which also affects the location of the B' band[23] or possibly to anharmonic effects.[22]

Nevertheless, platelets do not appear to arise as a result of electron irradiation of chemically pure type IIa diamonds,[24] even after anneals identical to those needed to create them in type Ib diamonds. This is a problem with the interstitial model which we shall return to. It would have been interesting to study the effect of *carbon* implantation into type IIa diamonds followed by annealing in the same way as the formation of extended self-interstitial defects in Si has been studied.

The platelet is unstable at a temperature (2400–2700 °C) and pressures where graphite is stable.[25] Under these conditions the platelets dissolve and perfect dislocation loops with Burgers vectors $\frac{1}{2}a_0\langle 011\rangle$ (Ref. 25) or $a_0\langle 100\rangle$ (Ref. 26) are formed. At the same time small octahedral voidites are formed which EEL experiments suggest contain nitrogen molecules under pressure. Hirsch *et al.*[26] suggested that the mechanism by which platelets shrink was the capture of vacancies, probably created by the anneal, and the transformation of the platelet into perfect dislocation loops, along with voidites, can be accomplished by interaction with a glide dislocation which generates Bardeen-Herring climb sources on the platelet.

Woods, however, was not the first to suggest the platelet is composed of interstitials. Using TEM, Humble[27] found a platelet lattice displacement, $\sim 0.4a_0$, which he thought too large to be explained by the Lang model. He then suggested that a larger displacement would arise if the nitrogen atoms in the Lang model are replaced by carbon, with pairing of the dangling bonds. This rebonding could be done in many ways but one of the basic units of the structure is a defect shown in Fig. 2(b), which was later recognized to be a complex of four self-interstitials denoted by I_4.[28] More recent TEM studies[12] show that the structure of {001} platelets along $\langle 011\rangle$ is different from $\langle 01\bar{1}\rangle$ but these differences could still be consistent with a rebonding of a layer of I_4 defects.[12] We have previously published theoretical studies regarding the energetics and intrinsic properties of perfect carbonacious platelets. There we showed that the Humble model is consistent with many experimental observations,[29,30] although the perfectly periodic structures cannot explain others, such as the low energy optical transitions. These previous calculations have also shown that carbonacious platelets are consistent with the location of the B' band:[29,30] the infrared active local vibrational modes of the tetrainterstitial complex [Fig. 2(b)] were found to lie at 1349, 1362, 1401, 1420, 1421, and 1569 cm^{-1}. They are close to bands at 1372, 1426, and possibly 1520 and 1540 cm^{-1}, assigned to platelets.[31]

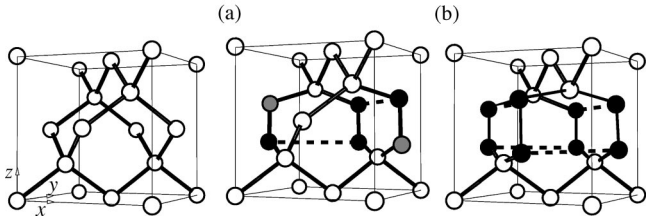

FIG. 2. Schematic of (a) the $O3$ center composed of three $\langle 001\rangle$ split interstitials, and (b) the Humble structure composed of four $\langle 001\rangle$ split interstitials. A section of pure diamond is also shown for comparison. The six (for $O3$) and eight (for the Humble defect) atoms forming the split-interstitial pairs are shaded, with the fully coordinated atoms in black and the threefold atoms in gray. The reconstructed bonds are indicated by the dashed lines.

The principal aim of the present study is explore the mechanisms driving the growth and, ultimately, the dissolution of these planar aggregates, with particular reference to the nitrogen aggregation process. We therefore examine the models of the platelet with reference to the energetics of nitrogen and self-interstitial aggregation using first principles modeling techniques.

As a byproduct of this study, we also find possible explanations for the spectroscopic characteristics of the platelets by deriving the electronic properties of disorder in the periodic platelet structures, i.e., from nitrogen impurities and ''vacancies.'' We shall show for the first time that the completely nitrogenous Lang model for the platelet is energetically unstable against the formation of *B* centers, and provide candidate structures of the nitrogen contaminants with the carbonacious structures.

We also expand upon the preliminary result reported previously,[29,30] with additional details regarding the phonon bands, the first report of theoretical electron energy loss spectra, as well as presenting for the first time the energies of alternative structures for extended interstitial defects based on those seen in silicon and germanium, *viz.* the {113} and {111} rodlike defects.

Since there is evidence that the platelet is a self-interstitial species, we briefly review in Sec. I A our understanding of self-interstitial defects. Section I B summarizes the theory of nitrogen aggregation, and Sec. I C describes, in greater detail, the results of experiments on platelets. We then describe our method in Sec. II and give our results in Sec. III. Finally, we report our conclusions in Sec. IV.

A. Self-interstitial aggregates

The planar self-interstitial defects can be best understood in the light of what is known about the smaller clusters of 1–4 interstitials, which we have previously examined in detail.[30,32] The structure of small self-interstitial clusters can

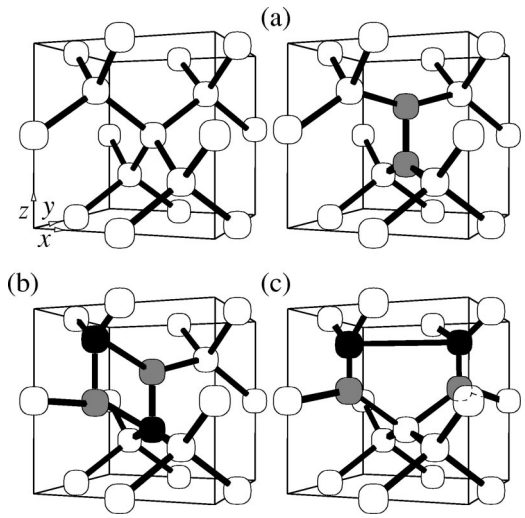

FIG. 3. Schematic of (a) the $R2$ EPR center assigned to a split-interstitial, (b) the $R1$ EPR center assigned to a close-by pair of split interstitials, and (c) the Humble ring di-interstitial where the two split-interstitials are separated by $a_0/\sqrt{2}$. A section of pure diamond is also shown for comparison. For (b) and (c), two of the atoms associated with each split-interstitial pair can be fully rebonded (shown in black) while the others each possess a single dangling bond (shown in gray).

be understood by considering first the isolated self-interstitial. This consists of a pair of atoms sharing a lattice site, bonded to the lattice, and aligned along $\langle 001 \rangle$. Thus there is a dangling bond associated with each atom sharing the lattice site, as shown in Fig. 3(a). When the spins of the electrons in each dangling bond are parallel the subsequent $S=1$ center has been identified with the $R2$ electron paramagnetic resonance (EPR) defect.[30,33] This structure of the single interstitial is readily appreciated as one which possesses the least number of dangling bonds.

Low energy forms of the di-interstitial arise when two I_1's are brought together in such a way to eliminate a pair of dangling bonds. This can be done in several ways. Figure 3(b) shows one way which has been associated with the $R1$ EPR center,[34] whereas another structure shown in Fig. 3(c) has been tentatively linked with the $3H$ optical center.[30,35] Both the $R1$ and Humble structures have been proposed as building blocks for the platelets.[27,36]

A tri-interstitial can be created by adding a third interstitial to the $3H$ form of I_2 shown in Fig. 3(c) in such a way that again only two dangling bonds survive. This C_2 defect is shown in Fig. 2(a) and has been assigned to the $O3$ EPR center which possesses the same C_2 symmetry.[30,37] A detailed calculation showed that the fine structure term found in magnetic resonance is in agreement with experiment. This family of self-interstitial aggregates, $R1$, $3H$, and $O3$, strongly suggests that the structure of the tetra-interstitial involves the addition of a further split-interstitial in such a way that all dangling bonds are eliminated. This defect is shown in Fig. 2(b) and has a D_{2d} symmetry. This defect may be formed when $O3$, created in *e*-irradiated diamond, anneals out around 450 °C.

The single self-interstitial and tetra-interstitial have formation energies around 12 and 5 eV per interstitial, respectively.[30,32] This enormous reduction is due to the elimination of dangling bonds and the residual energy reflects the strain energy of the defect. These formation energies imply that the equilibrium concentrations of the interstitials will be negligible and they can only be produced through irradiation, implantation or as the result of the aggregation of impurities such as nitrogen.

At first sight, it might be thought that the latter process could lead to the kick-out of self-interstitials in the same way as oxygen precipitation in Si generates silicon-interstitials. Although there are parallels between the two processes, as both involve the creation of vacancy-impurity defects, the essential difference resides in the interstitial nature of oxygen in Si and thus strain-reduction plays an important role in the creation of the self-interstitial.[38] In the case of diamond however, strain may not play such an important role[32] as the volume expansion of substitutional nitrogen and nitrogen aggregates in diamond is similar or smaller to that of interstitial oxygen in silicon. Moreover, there are great differences between diamond and silicon in the relative formation energies of self-interstitials and vacancies: the formation energies of vacancies and interstitials in Si are believed to be roughly equal [$\sim 3-4$ eV (Refs. 39–42), whereas in diamond the vacancy has a formation energy of ~ 6 eV,[43] and, as stated above, the self-interstitial is twice that value at 12 eV.

B. Nitrogen aggregation

As stated above, {001} platelets are formed in diamond when nitrogen dissolved in the lattice aggregates. It is generally believed that the interstitial species that ultimately form platelets arise from this nitrogen aggregation process, and it is therefore of key importance to understand the energetics of the nitrogen aggregation processes. There is a considerable literature dedicated to nitrogen aggregation and the properties of the aggregates themselves, and we therefore summarize here only the main points pertinent to the platelet problem.

Annealing type Ib diamonds, $[N_s] \sim 10^{20}$ cm^{-3}, around 2000 K, results in the first stage of nitrogen aggregation when nearest neighbor pairs, labeled A centers, are formed.[21,24,44] Thus

$$N_s + N_s \rightarrow A,$$

where N_s is the isolated substitutional N defect. The A center is depicted schematically in Fig. 4(a). The formation of A centers is sometimes accompanied by the formation of complexes of a vacancy with two nitrogen atoms [VN_2, Fig. 4(b)] which gives rise to the optical peaks labeled $H2$ and $H3$. The activation energy for the growth of A-centers has been experimentally found to be ~ 5 eV.[21]

At temperatures above 2500 K, the A centers anneal out and B centers are formed. The B center is a complex of four nitrogen atoms and a lattice vacancy [VN_4, Fig. 4(c)].[18] One mechanism in which B centers are formed involves the diffusion of A centers and the kick out of an interstitial when two A centers react:

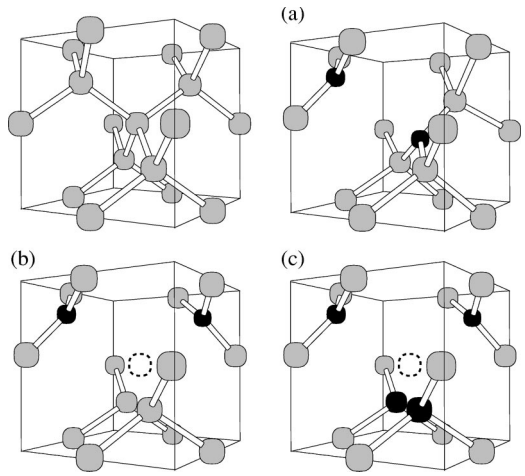

FIG. 4. Schematic representations of the nitrogen aggregates. (a) the *A* center composed of a neighboring pair of substitutional N atoms, (b) VN_2 or $H3$ center, and (c) VN_4 or *B* center. Gray and black atoms represent carbon and nitrogen, respectively. The dashed circle indicates the location of a vacancy. A section of bulk material is also shown for comparison.

$$A + A \rightarrow B + I, \tag{1}$$

with I representing the self-interstitial. At temperatures where *B* centers are formed, the self-interstitial is mobile and can be trapped at sinks such as the surface, dislocations and platelets.

Alternatively, *B* centers can be formed without the production of an interstitial. Thus *A* centers could trap thermally generated mobile vacancies, and form a relatively mobile VN_2 species ($H3$ defect). *B* centers can then be formed directly in the reactions:

$$A + V \rightarrow H3 \quad \text{and} \quad A + H3 \rightarrow B. \tag{2}$$

Other possible mechanisms exist such as the dissociation of the *A* center and the formation of first *V*N, followed by other VN_n species and ultimately by *B* centers. Some support for this mechanism comes from the observation of VN_3, assigned to the N3 optical center, when *B* centers are formed.[15] However, such defects are in the minority and the main products are *B* centers and nitrogen defects within platelets.

All these mechanisms lead to the formation of *B* centers but only the first, in Eq. 1, leads to the formation of *self-interstitials*. The observations of vacancy centers along with *B* centers gives support to the latter reactions being dominant but then leaves a major gap in our understanding as to the origin of the self-interstitials which aggregate to form platelets. We shall return to this problem below but note here that the activation energy for the production of *B* centers has been crudely estimated in the annealing experiment to be ~ 7 eV.[21]

C. Platelets: experimental data

1. Transmission electron microscopy

Platelets were first observed in TEM by Evans and Phaal in 1962,[5] but until relatively recently the resolution was insufficient to determine their core structure.[8,12] The TEM micrographs typically show {001} platelets as rectangular objects with edges aligned along the $\langle 110 \rangle$ and $\langle 1\bar{1}0 \rangle$ directions, although irregularly shaped platelets are also seen. A crucial observation is that the $\langle 110 \rangle$ and $\langle 1\bar{1}0 \rangle$ directions in the plane of the platelet are *inequivalent*.[8] In some cases a weak periodicity of close to $\sqrt{8}a_0$ is seen in the $\langle 110 \rangle$ direction.[8]

The dilation of the lattice perpendicular to the plane of the platelet has been measured to be $0.33a_0$ (Ref. 8) and $0.39a_0$ (Ref. 9) for 20–30-nm and 1-μm platelets, respectively. These values agree well with the early estimates[4] from the x-ray diffraction ($0.34a_0$) and the large-angle convergent-beam electron diffraction technique[10] which yielded a value of $0.40a_0$ for a large (1-μm) platelet. The size dependence of the lattice dilation is probably related to edge effects and the value of $0.40a_0$ for larger platelets is believed to be consistent with models based on carbon interstitials,[10] such as that proposed by Humble.[27]

2. Optical activity

Platelets have been associated with a broad luminescence band[45,46] centered at 1.25 eV (990 nm), which impairs the efficiency of optical windows made from natural diamonds. For 'giant' platelets it has been shown that this absorption band is strongly polarized with the electric field lying in the plane of the platelet.[2] High energy absorption and luminescence bands around 4.6 and 4.4 eV (270 and 280 nm) (Ref. 16) are also linked to platelets. The intensities of the 990 nm (1.25 eV) and 280/270 nm (4.4/4.6 eV) bands are related to the intensity of the B' band.[47] Other transitions have been tentatively linked to platelets. A broad luminescence around 580 nm (2.14 eV) has been linked to the platelet, or a point defect located near it.[48] VN_3 defects which luminesce at 2.985 eV (the $N3$ band) has been detected in the vicinity of 'giant' platelets. Their polarization is the same as that exhibited by the broad-band luminescence, taken to imply a pronounced local strain.[48] Differences between the N3 transition in the presence of platelets and those in the lattice have been interpreted in terms of a local narrowing of the band gap.[49] A zero phonon line at 491 nm also exhibits a strong polarization, but only in material containing platelets.[48]

It is clear that the compressive strain caused by the platelet could attract vacancy defects leading to a number of broadened optical transitions. It would have been interesting to follow the evolution of the optical bands when ''man-made'' platelets are formed and also the changes caused by platelet dissolution and the formation of dislocation loops.

As mentioned above, the B' infrared absorption band around 1370 cm^{-1} has been connected with platelets. The position of B' increases with the size of the platelet,[23] but lies in the range 1358–1378 cm^{-1}. This shift may be due to an increasing displacement, and hence strain, in larger platelets or it may reflect a change in nitrogen composition.[15]

The B' band is accompanied by other IR-absorption features, notably one at 328 cm^{-1} and a number of local modes measured at 1426, and possibly 1520 and 1540 cm^{-1}.[31] Previous modeling has associated the 328-cm^{-1} band to a bend

mode of a single nitrogen species.[20] This defect anneals around 2300 °C where platelets are stable and cannot then play an essential role in the structure of the platelet.[14]

3. Electron energy loss spectroscopy

Electron energy loss spectroscopy (EELS) has shown[11–14] that nitrogen is present in detectable concentrations in most platelets. However, the concentration varies dramatically, lying between 6% and 61% of a monolayer.[12–14] The fact that the nitrogen concentration is so variable suggests that it is an adventitious contaminant rather than constituting an essential component of the structure. A low concentration is consistent with the insensitivity[22] of the B' band in diamonds containing platelets and doped with ^{15}N.

EEL spectroscopy also provides information regarding the local bonding configuration of N in the platelet. The nitrogen *K*-edge threshold suggests that nitrogen is bound in a 'diamondlike environment'.[13] However, the precise bonding configuration is uncertain. Kiflawi *et al.*[14] state that the similarity in the C- and N-related *K*-edge spectra imply that they have similar bonding configurations. However, a detailed examination of the *K*-edge onset suggests that the nitrogen is in the form of N pairs.[50] This would imply that N in the platelet is in a different environment from carbon since the A'-center possesses a dilated N-N bond, rendering the N atoms essentially threefold coordinated.[32]

There have been no reports to date of low-loss EEL studies which provides information on dipole allowed transitions between occupied and unoccupied electronic states in the vicinity of the band edges. In anticipation that such results will soon become available, we investigate theoretically the low-loss EELS spectrum of platelets in Sec. I C 3.

4. Interstitial related extended defects in other materials

Interstitial related $\langle 100 \rangle$ platelets have been found following deuteron-implantation and high temperature anneals in Ge (Ref. 51) and occasionally in Si.[52] However, the more common extended interstitial defects both in Si and Ge are rodlike defects (RLDs), which are aligned along $\langle 1\bar{1}0 \rangle$ and inhabit {113} planes,[41,53–57] and {111} planes.[58–60] RLDs have been extensively studied by a combination of TEM and theoretical modeling. The structure of the {113} and {111} rodlike defects is presented schematically in Figs. 5, 6, and 7. The core of the defect [Fig. 5(a)] is made from a chain of self-interstitials inserted into a $\langle 1\bar{1}0 \rangle$ channel. The chain is bonded into the lattice so that each atom is fourfold coordinated, except the ones at the end. The simplest rebonding is shown in Fig. 5(a) but further distortions, involving bond switching must occur to account for a {113} habit plane. These are shown in Figs. 5(b) and 5(c). Finally, the separation of chains in the {113} plane must be considered. Figs. 6(a)–6(c) show some of the models that have been suggested for silicon. The formation energy per interstitial in the RLD, as estimated by a tight binding method for silicon, is 1.3 eV, compared to the formation energy of a single isolated interstitial of 3.9 eV.[41] This shows that a single interstitial is bound to the RLD by 2.6 eV.

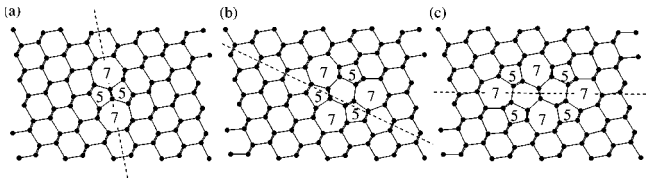

FIG. 5. Schematics of the core of the linear {113} defect observed in silicon and germanium projected onto the $(1\bar{1}0)$ plane. The vertical and horizontal axes are [113] and $[\bar{3}32]$ respectively. (a) shows the structure generated by the insertion of a single $[1\bar{1}0]$ chain where the rebonding with the lattice results in adjacent five-member rings. (b) after one bond-switch the five-member rings are separated. (c) shows the structure after a second bond switch, the basis of the {113} defect. Five- and seven-member rings are shown explicitly.

In Si, the bulk of RLDs inhabit a {113} plane, but a minority ($\sim$10–15 %) lie in a {111} plane.[58–60] The structure of these is not completely understood but they possibly involve $\langle 1\bar{1}0 \rangle$ chains lying in a {111} plane,[60] as shown in Fig. 7. This structure can be understood in terms of an aggregate of the primitive $\langle 110 \rangle$ chains shown in Fig. 5(a) in the habit plane shown by the dashed line.

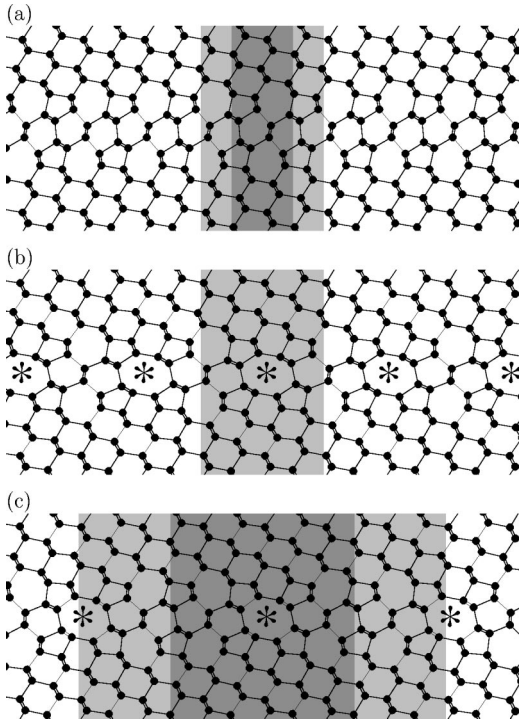

FIG. 6. Schematics of three varieties of a periodically continued set of $\langle 1\bar{1}0 \rangle$ chains which form a {113} planar defect, projected onto the $(1\bar{1}0)$ plane. The vertical and horizontal axes are [113] and $[\bar{3}32]$ respectively. The light-shaded areas indicate one period of each structure, and, for structures (a) and (c) the darker shaded area shows the apparent periodicity where it differs from the actual period. The aggregates can be described by their apparent periodicity as (a) /*I*/, (b) /*IO*/, and (c) /*IIO*/, where *I* represents the single chain shown in Fig. 5(c), and *O* an "empty" $[1\bar{1}0]$ channel which forms an eight-member ring, indicated by an asterisk.

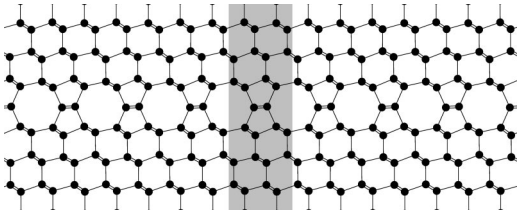

FIG. 7. Schematic structure of a {111} planar interstitial aggregate, projected onto the $(1\bar{1}0)$ plane. The vertical and horizontal axes are [111] and $[11\bar{2}]$, respectively. The periodicity is indicated by the gray band.

There is no evidence that {113} defects occur in diamond, but {113} and {001} platelets coexist in germanium[51,52] suggesting that, at least for this material, these structures are competitive in energy. The difference in interstitial platelets in diamond from those in Si and Ge is striking and will be investigated in Sec. III E.

D. Planar interstitial aggregate models

Many microscopic models for platelets have been proposed, but we shall confine our discussion to purely carbonaceous models given the lack of evidence, as explained above, for a nitrogenous species. The basis of the carbon models for the platelets can be understood in terms of the model first proposed independently by Humble[27] for diamond and Ferreira-Lima[61] for germanium. Most simply this involves a {001} layer of tetrainterstitial defects as illustrated in Fig. 2(b). Humble suggested that the platelets would be made up from some arrangement of these fully coordinated I_4 building blocks, but has since been misrepresented as proposing a model with perfect tetragonal symmetry[8] illustrated schematically in Fig. 8(a).

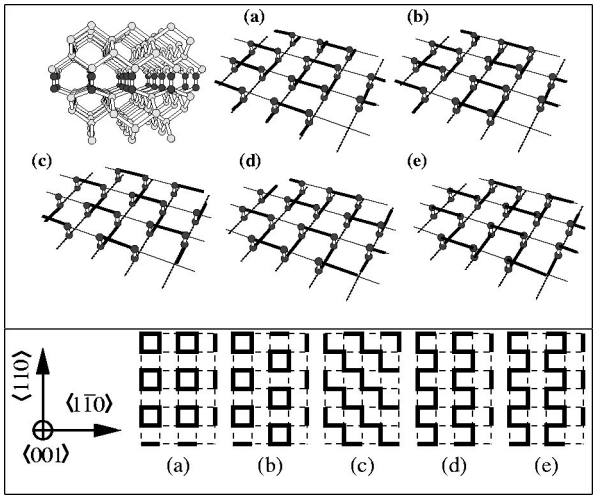

FIG. 8. Candidate structures for the platelet based on the model of Humble (Ref. 27). Upper panel, top left shows a section of bulk material where a single {001} layer of atoms has been replaced with ⟨001⟩-oriented split-interstitials shown in black. Each atom in the split-interstitial pair has a dangling bond lying in the {001} plane parellel to either [110] or $[1\bar{1}0]$ (not shown). The other diagrams show only the (001) plane of split interstitials where the dangling bonds have been paired in different ways. Each reconstructed bond is shown as a full black line. The two sets of dotted lines show the [110] and $[1\bar{1}0]$ directions. (a) and (b) are different arrangements of tetra-interstitials where the [110] and $[1\bar{1}0]$ directions are equivalent in (a) but not in (b). This is most easily seen by checking for a [010] reflection plane. (c)–(e) consist of [010], [110] and $[1\bar{1}0]$ chains of reconstructed bonds. The [110] and $[1\bar{1}0]$ directions are equivalent in (c) but not in (d) and (e). The lower panel shows a (001) projection of the reconstructed bonds where the equivalence of the ⟨110⟩ directions in (a), and (c) is more apparant.

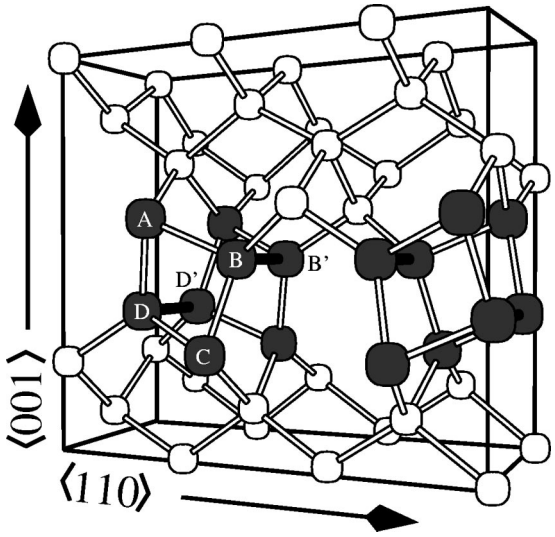

FIG. 9. A schematic representation of the unit cell of the $R1$-platelet model. The reconstructions between "$R1$" centers [$ABCD$, see Fig. 3(b)] lead to the elimination of dangling bonds and are indicated by black bonds (e.g., B-B' and D-D').

Several structures based on the Humble model have been used as the basis for comparison with the TEM micrographs.[8,12] The simplest Humble model [Fig. 8(a)] can be discounted due to the equivalence of its ⟨110⟩ and ⟨110⟩ projections. Also, the presence of a C_2 ⟨001⟩ axis for the reconstruction depicted in Fig. 8(c) shows that the ⟨110⟩ and $\langle 1\bar{1}0\rangle$ projections are equivalent, in conflict with TEM studies.[8] Therefore these two models cannot then be correct. However, as noted by Humble, the bonds in each I_4 unit can be broken and rebonded with neighboring units yielding many different models. Figures 8(d) and 8(e) show sets of parallel bonded chains along $\langle 1\bar{1}0\rangle$, and along with the model illustrated in Fig. 8(b) are asymmetric between these projections. Any of these is a possible model for a periodic platelet structure, although a combination of all these topologies might well occur in practice.[12] Such disordered structures would satisfy the TEM observation that there is only a very weak periodicity along ⟨110⟩. Disorder will most likely introduce high-energy, unsatisfied carbon bonds, but the incorporation of nitrogen at such sites would remove these.

Another model constructed from aggregated $R1$ di-interstitial defects has been suggested[36] and is shown in Fig. 9. This $R1$ platelet has a higher density of interstitials than the Humble forms and consists of ⟨001⟩ split-interstitials condensed onto *two* {001} planes. In this model pairs of $R1$ defects, shown schematically in Fig. 3(b), reconstruct by

forming bonds between pairs of three-fold coordinated C atoms, in a similar way to the Humble model.

II. METHOD

The results described below were obtained using the local-density-functional technique as implemented in AIMPRO.[62,63] This allowed us to evaluate the energies and structures of platelets and related defects in large supercells. To model {001} platelets, unit cells containing 16 {001} layers of atoms, with 4, 8 or 16 atoms per plane depending on the periodicity of the platelet model have been used. For {111} defects, cells with lattice vectors along $\langle 111\rangle$, $\langle 1\bar{1}0\rangle$, and $\langle 11\bar{2}\rangle$ containing 9 and 12 {111} planes of atoms were constructed. Finally for the {113} oriented structures, the lattice vectors of the supercell are chosen to lie along $\langle 113\rangle$, $\langle 1\bar{1}0\rangle$, and $\langle 33\bar{2}\rangle$. The basic unit cell contains 44 bulk atoms. The calculations have been performed using the Monkhorst-Pack[64] scheme for sampling the Brillouin zone. In each case the results quoted have been converged with respect to the number of k points.

Norm-conserving pseudopotentials[65] enabled core electrons to be eliminated. The wavefunction basis consists of independent s, p_x, p_y and p_z Gaussian orbitals with four different exponents, sited at each C, Si, or N site. In addition, a set of s and p Gaussian orbitals was placed at each bond center. The charge density is Fourier transformed using plane waves with a cutoff of 120 Ry. The dependence of the results on the basis set was investigated by using an alternative basis composed of three independent sets of s and p Gaussian orbitals with one set of s, p, and d orbitals centered at each atomic site. The lattice constant and bulk modulus of diamond using these bases are within $\sim 1\%$ and 5%, respectively, of the experimental values, while the direct and indirect band gaps are close to previously published plane-wave local density approximation values[66] (5.68 and 4.18 eV).

The formation energy $E^f(X)$ of a defect X made up from atoms with chemical potentials μ_i is given by

$$E^f(X) = E(X) - \sum \mu_i .$$

Here $E(X)$ is the total energy of the supercell containing the defect, and the sum is over all atoms in the supercell. For a supercell of n carbon atoms containing a platelet consisting of N carbon interstitials, the formation energy per interstitial is given by

$$E_I^f(P) = \frac{E(P) - n\mu_C}{N}, \tag{3}$$

where $E(P)$ is the total energy of the platelet supercell and μ_C is the chemical potential of carbon, taken to be the energy per atom of bulk diamond. The formation energies defined in this way allow us to compare defects containing different numbers of interstitials, vacancies, or even nitrogen atoms. The formation energy is a thermodynamic free energy, evaluated at 0 K and zero pressure, and controls the concentration of defects in equilibrium with reservoirs of carbon or nitrogen species.[67]

TABLE I. Relative formation energies per N atom (E^f_N, eV) for substitutional nitrogen N_s, N pairs, and vacancy nitrogen defects (neutral charge states). The zero of energy is taken to be the lowest energy structure: the VN_4 (B center).

Defect	N_s	$(N_s)_2$	VN	VN_2	VN_3	VN_4
E^f_N	2.9	0.9	5.4	1.8	0.6	0.0

The vibrational modes of the platelets are calculated by finding the energy second derivatives between atoms in the core of the defect directly from AIMPRO and using a Musgrave-Pople valence force potential potential to evaluate the derivatives with the remaining atoms.[68] From these data a dynamical matrix can be constructed and the normal modes found in the usual way.

EELS simulations were carried out using the approach described elsewhere.[69] This technique has previously been applied to dislocations in diamond.[70] For the spectra reported here, the conduction bands are shifted upwards by 1.48 eV to bring the calculated gap into agreement with the experimental one. The transitions have been broadened using a Gaussian of width 0.8 eV and the Brillouin zone is sampled approximately uniformly with a density of the order of 10^{-5} Å^3, which typically requires a few hundred k points.

III. RESULTS

A. Energetics of nitrogen aggregation

We first describe the energetics of the two stages involved in nitrogen aggregation. We incorporated the defects in 64-atom cubic unit cells, and allowed all atoms to move until an equilibrium structure resulted. The volume of the cell was kept fixed and the formation energies of the neutral substitutional N defect (N_s), A center, and B center, found. These are given in Table I. Contributions to the formation energies of these defects caused by allowing the volume of the supercell to relax are known to be small.[32] The structures of these defects are in agreement with those found previously,[19] and the binding energies are generally consistent with previous *ab initio* calculations.[71]

The binding energy (E^b) of the nitrogen atoms in the A center is given in terms of the formation energies by

$$E^b(A) = 2E^f(N_s) - E^f(A).$$

Here, in analogy to Eq. (3), the formation energies of N_s and the A center in the 64-atom cells are given by

$$E^f(N_s) = E(N_s) - \mu_N - 63\mu_C,$$

$$E^f(A) = E(A) - 2\mu_N - 62\mu_C.$$

Previous investigations[72] show that μ_N derived from a gas of nitrogen molecules is very small accounting for the high solubility of nitrogen in diamond. In the following we refer only to binding energies of nitrogen in various defects

and these energies are independent of μ_N. Table I shows that the binding energy per N atom in the *A* center to be around 2 eV and about a factor of 2 greater than found in a previous semiempirical study,[73] but in agreement with other density functional calculations.[71]

There are three simple mechanisms by which impurities diffuse. Two of these first require the impurity to trap a thermally generated vacancy or interstitial. This is followed by a reorientation of the defect transferring the impurity to a different lattice location within the vacancy or interstitial complex. Finally, the intrinsic defect is emitted leaving the impurity in a different lattice location from the starting one. The third mechanism involves a concerted exchange of the impurity with a neighboring lattice atom, without the need for a vacancy or interstitial. The activation energy for the first two processes is expected to be close to the sum of the formation and migration energies of the intrinsic centers. Even if a vacancy can be formed adjacent to nitrogen with a lower formation energy, we would expect the diffusion energy of nitrogen to be close to that of self-diffusion via a vacancy mechanism,[40] provided that the species were neutral. The formation energy of the vacancy is very difficult to treat precisely due to the complicated multiplet nature of the vacancy electronic structure. A value of $E^f(V)$ equal to 6 eV is found from quantum Monte Carlo methods.[43] A single determinental wavefunction in density functional theory gave almost 7 eV. The vacancy migration energy has been estimated previously[74] to be 2.8 eV in reasonable agreement with experimental data (2.3 ± 0.3 eV).[75] The activation energy for nitrogen diffusion by a vacancy mechanism would then be around 8–9 eV.

The interstitial formation energy is found to be 12.3 eV as discussed above and its migration energy about 1.7 eV.[74,76] The gives a diffusion energy via an interstitial mechanism of at least 14 eV which is clearly much greater than the 8–9 eV found for a vacancy mechanism. However, the experimental value for the activation energy for the formation of *A* centers is around 5 eV. This suggests to us that a concerted exchange process for nitrogen diffusion is favored.

Let us now consider the energy change, E^e, in the reaction where a *B* center is formed from two *A* centers.

$$E^e(B) = E^f(B) - 2E^f(A).$$

Here the formation energy of the B center in the 63 atom cell is given by:

$$E^f(B) = E(B) - 4\mu_N - 59\mu_C.$$

From Table I, the energy change $E^e(B)$ is -3.8 eV and this includes the energy necessary to create the vacancy in the *B* center. Thus the reaction

$$A + A \rightarrow B, \tag{4}$$

is exothermic, and *A* centers are unstable in the diamond lattice, spontaneously creating *B* centers.

Although the energies of the interstitial or vacancy are not involved in the enthalpy change in reaction Eq. (4), they are required to estimate the *activation barrier* for the production of *B* centers. Since the formation and migration energies of an isolated interstitial are 12.3 eV and 1.7 eV, respectively,[30,74,76] the barrier in Eq. 1 must be at least 10.2 eV which is considerably larger than the experimental estimate of 7 eV.[21] The interstitials formed in the process are able to diffuse until trapped by a growing platelet. However, this implies the binding energy of a self-interstitial with the platelet must exceed 12.3–3.8 or 8.5 eV in order that the net process is exothermic. This binding energy has implications for the platelet structure.

The activation energy involved in the vacancy mechanism of Eq. (2) is again expected to be dominated by the vacancy formation and migration energies or 8–9 eV. This is somewhat smaller than the barrier for interstitial production and conflicts with the view that interstitials are produced along with *B* centers according to Eq. (1).

It is our belief that isolated interstitials are *not* produced. It is instructive to consider the platelet not as an inserted plane of interstitials but as a partial dislocation loop, lying on a $\{001\}$ plane, with a Burgers vector $\langle 00R \rangle$ where R is the displacement $\approx 0.4a_0$. The growth of the loop occurs by climb which must release vacancies. These vacancies then lead to *B* centers via Eq. (2). Our model for the platelet to be discussed in Sec. III B considers it to be an aggregate of I_4 defects. A jog at the perimeter can be considered to be the replacement of I_4 locally by the I_3 defect. At any temperature there will be a distribution of these around the perimeter of the platelet. The climb occurs by (a) the creation of an interstitial-vacancy pair at the platelet, (b) the binding of the interstitial to the jog extending the platelet by converting I_3 into another I_4 unit, and (c) the vacancy diffusing away. The energy for (a) can be considered to be the formation energy of a Frenkel pair consisting of an interstitial and vacancy at the platelet. These will be shown below in Secs. III B 1 and III D to be about 1 and 4.5 eV, respectively. Thus the Frenkel pair at the platelet has a formation energy of 5.5 eV and is less than the formation energy of a single vacancy in bulk. For (b) the energy lowering on moving the interstitial from the platelet to a jog on the bounding dislocation is approximated by the difference in formation energies of an isolated I_4 on one hand, and the sum of the formation energies of an isolated I_3 on the other together with the formation energy of I_1 at the platelet. This assumes that the effect of stress due to the remaining platelet is the same for I_4 and I_3. Now, the formation energies of I_4 and I_3 are roughly equal[30] thus leaving the binding energy of the interstitial with the jog to be ~ 1 eV. For (c), the activation barrier to the vacancy diffusing away from the dislocation is the binding energy of the vacancy with the platelet plus the migration energy of the vacancy in bulk. The binding energy is simply the difference between the vacancy formation energies in bulk and at the platelet and is thus about 1.5–2.5 eV This gives the activation barrier for the vacancy to move away from the platelet to be $\sim 4.3 \pm 0.5$ eV.

Thus the activation energy for the creation of the vacancy and interstitial at the platelet, for climb of the jog, and to diffuse the vacancy away from the platelet, is about $4.5 + 1 - 1 + 4.3 \pm 0.5$ eV or 8.8 ± 0.5 eV. This estimate is somewhat above the, admittedly crude, experimental value of ~ 7 eV but the point is that the process also leads to the creation of

TABLE II. Formation energies per interstitial (E^f, eV) for the various platelet models [(a)-(e) in Fig. 8 and the $R1$ platelet of Fig. 9] for the bulk lattice constant and for the volume relaxed unit cell. In the latter case the displacement along $\langle 001 \rangle$ is also quoted.

		Model					
		(a)	(b)	(c)	(d)	(e)	$R1$
Unrelaxed along $\langle 001 \rangle$	E^f	3.58	3.69	4.01	3.82	3.75	4.16
	E^f_I	1.04	0.90	1.27	1.20	1.14	2.15
Relaxed along $\langle 001 \rangle$	Displacement/a_0	0.38	0.37	0.37	0.38	0.38	0.37

an interstitial at the platelet and hence is a mechanism for platelet growth. The important conclusion is that platelets grow from the release of thermally generated vacancies from the bounding dislocation and their trapping by A-centers and not from a condensation of interstitials. This immediately explains why they do not arise from electron irradiation of type II diamond in the same way as the growth of extended interstitial defects in irradiated silicon. The process is also different from oxygen precipitation in Si.

B. Periodic carbonaceous {001} planar models

1. Energetics of self-interstitial aggregation

Table II gives the formation energies per interstitial of the five models of the {001} planar interstitial platelet shown in Fig. 8, repeated from Ref. 30 with the addition of the R1-platelet illustrated in Fig. 9. The latter has a higher energy than any of the models based on Humble tetra-interstitial complexes and can be discarded. The table records the energy both when the z axis of the unit cell is held fixed to the value for bulk diamond and when this is allowed to relax (see Sec. III B 2). Inserting a plane of interstitials necessarily leads to a displacement along z which does not vanish in the limit of an infinite cell. Unphysical results can then arise if this effect is ignored. Table II shows that the effect of relaxation is very large with energies dropping by more than a factor of three. The most stable structure is (b), although the range of formation energies for the various Humble models is less than 0.4 eV.

We present here the effect of the basis and unit cell size. First we repeated the calculation for model (a) in the same size unit cell with the alternative basis outlined in Sec. II. The formation energy per interstitial is only 4% higher than that quoted in Table II. Second, increasing the size of the unit cell by 50% in the direction normal to the plane of interstitials had less than 1% effect on the formation energy per interstitial. We conclude from these calculations that the unit cells and basis we have used provide us with sufficiently converged results.

The energy per interstitial in the platelet should be compared with the energies of small aggregates. The formation energy of a single interstitial, the $R2$ EPR center described above, is around 12 eV. For the tetra-interstitial, this drops to around 5 eV per interstitial and to about 0.9 eV for the most stable platelet model shown in Fig. 8(b). Thus there is a considerable saving in energy in platelet formation. Specifically, the binding energy of an interstitial to a large platelet is the difference between 12 and 0.9 eV. This is more than sufficient to make the transformation of A centers into B centers, along with platelets, according to Eq. (1), exothermic. The minimum formation energy of 0.9 eV per interstitial corresponds to a surface energy of 40 meV Å^{-2} which is about twice that of an intrinsic stacking fault: 17.8 ± 2.5 meV Å^{-2} (Ref. 77). This fault arises purely by shear and does not contain any interstitials.

The various models shown schematically in Fig. 8 chiefly differ from each other in their projected structures along the $\langle 110 \rangle$ and $\langle 1\bar{1}0 \rangle$ directions. For the model to be a candidate for the platelet, the projections must differ from each other. In Fig. 10 we show the projections of the various models along the $\langle 110 \rangle$ directions in line with the previous experimental reports such as those of Humble *et al.*,[78] Barry,[79] and

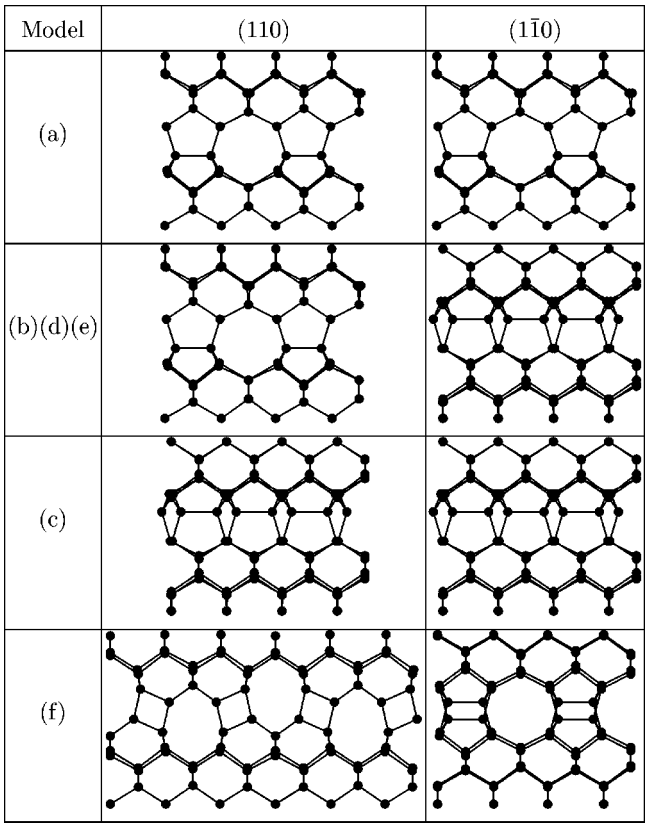

FIG. 10. Projections onto the (110) and (1$\bar{1}$0) planes for the six models depicted in Fig. 8. The vertical direction is $\langle 001 \rangle$ in all cases. Only structures for which the two projections are inequivalent are candidates for the {001} platelets in diamond.

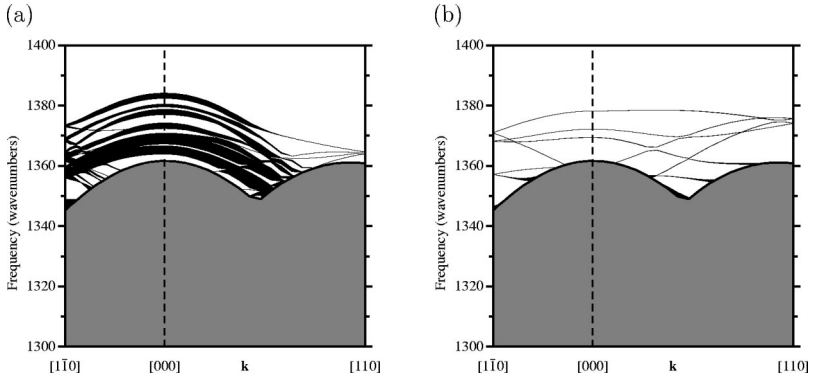

FIG. 11. Vibrational (phonon) bands of bulk diamond projected on the {001} plane (shaded area) and high-energy vibrational bands localized in the {001} plane of the platelet shown in Fig. 8(b) (black lines). The dispersion for frequencies around the Raman frequency is shown along $\langle 110\rangle$ and $\langle 1\bar{1}0\rangle$ directions (normal to the platelet) in the folded Brillouin zone. (b) shows that relaxation of the cell along its normal has little effect on the frequencies but reduces their localization to the platelet.

Fallon *et al.*[12] Such projections are useful for the interpretation of structures viewed in high resolution TEM. For the structure to be a candidate for the platelets the projections must differ. Therefore configurations (b), (d), and (e) all satisfy this requirement. The $R1$ platelet model is also shown in Figs. 10, and this too gives rise to inequivalent $\langle 1\bar{1}0\rangle$ and $\langle 110\rangle$ projections. Configuration (b) then is our favored model, although the small energy difference between (b) and (a) suggests that random mixtures of these structures may coexist.

Large platelets would be unstable against the formation of a perfect dislocation loop. For a loop of radius r, the platelet energy varies as r^2 whereas that of a prismatic perfect loop varies as $r\ln r$. We can estimate the radius r of a platelet whose energy E_p equals that of a perfect dislocation loop where the interstitials have rearranged themselves as follows. We suppose that the single layer of interstitials in the platelet are moved to form *four additional* planes in a loop of Burgers vector $a_0\langle 100\rangle$ and of radius $r/2$ or two additional planes planes for loop with Burgers vector $a_0\langle 110\rangle/2$ of radius $r/\sqrt{2}$. Such loops have the same stacking sequence as bulk diamond[25,26] and are bounded by perfect dislocations. The energies of the platelet, $a_0\langle 110\rangle/2$, and $a_0\langle 100\rangle$ dislocations, (E_d^{110} and E_d^{100} respectively) are, respectively, for a platelet radius r:[80]

$$E_p=\frac{\mu(0.4a_0)^2 r}{2(1-\nu)}\left[\ln\left(\frac{4r}{\rho}\right)-1\right]+\pi r^2\gamma,$$

$$E_d^{110}=\frac{\mu a_0^2 r}{8\sqrt{2}(1-\nu)}\left[\left(2-\frac{\nu}{2}\right)\ln\left(\frac{4r}{\sqrt{2}\rho}\right)-(3-\nu)\right],$$

$$E_d^{100}=\frac{\mu a_0^2 r}{4(1-\nu)}\left[\ln\left(\frac{2r}{\rho}\right)-1\right].$$

Here, γ is the formation energy per unit area of the platelet, μ is the shear modulus (536 GPa), ν is Poisson's ratio for diamond (0.068), and ρ is the core radius of the dislocation (in each case taken to be the magnitude of the Burgers vector, where the Burger vector for the platelet is taken to be $0.4\,a_0$). The platelet is lower in energy than the {110} structure up to around only 6–7 nm and the {100} loop is lower in energy above around 40 nm. These radii are relatively insensitive to the values of ν, μ, and even γ: for example, it requires a drop of orders of magnitude in γ to yield a stability for the platelet up to the order of hundreds of nm, the typical length scale seen in TEM. The implication is then that the platelets are metastable owing their existence to kinetic factors probably related to the difficulty of transforming to perfect dislocation loops. Such a transformation however apparently readily occurs in the graphite stable region where the lattice is unstable. Mechanisms for this degradation have been discussed[26] and are not inconsistent with our mechanism for platelet growth.

2. Platelet displacement

As described in Sec. II, the supercells used to simulate the structures in Figs. 8 and 9 possess 16 host atomic layers plus one additional layer of interstitials, all contained within a period initially taken to be $4a_0$ along $\langle 001\rangle$. To study the displacement, for each unit cell the {001} cross section is fixed and the $\langle 001\rangle$ dimension expanded. The atoms in the supercell are then relaxed and the energy evaluated as a function the displacement vector. The profiles are very similar for all of the models, revealing a substantial drop in the total energy of $\sim$2.5–2.8 eV per interstitial, lowering E_I^f for this structure to just 0.9–1.3 eV. For each model we have evaluated the displacement vector which minimizes the total energy. For large platelets where edge effects are not significant, the measured displacement R is simply the lattice dilation of the supercell. For smaller platelets the boundary would tend to constrain the dilation of the lattice yielding a smaller value for R, consistent with the correlation of the measured dilation with platelet size.[10] The calculated displacements[81] listed in Table II are remarkably similar for all the models, and close to the upper limit of the experimental values. The implication is that, although the models are consistent with experimental observations, this parameter cannot be used to discriminate between different models. Finally, to check the sensitivity of the result with basis size, we repeated the calculation with the alternative basis set described above, finding less than a 1% variation.

3. Electronic and optical properties

We now extend our previous investigation of the infrared activity of the platelet.[29,30] The dispersion of the vibrational modes for the various models of platelet all exhibit qualitatively the same behavior. The projected bands for the structure of Fig. 8(b), with and without z-axis relaxation, are plotted in Fig. 11. It is clear that the platelet introduces modes

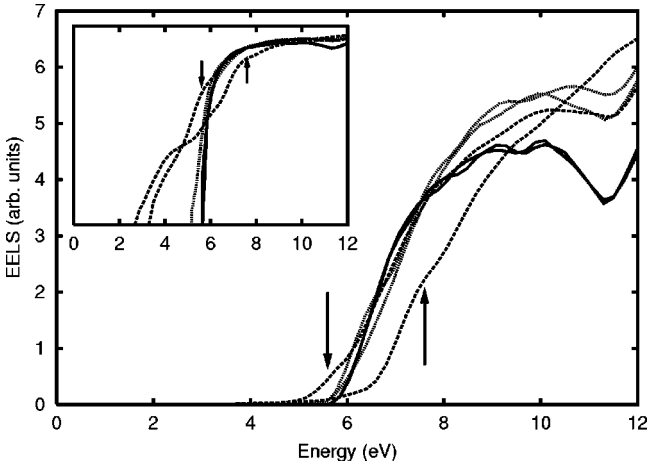

FIG. 12. Calculated low-loss EEL spectrum for the platelet when the cell is relaxed normal to the platelet (dotted line) and when constrained to the diamond lattice parameter (dashed line). The solid line represents the EEL spectrum for bulk diamond using the same size unit cell and sampling as used for the platelets. This was shifted to give a direct band gap of 6 eV. The inset is the same plot with a logarithmic scale to reveal the tails in the band-gap. The up-arrow symbol indicates the spectrum for the volume constrained cell when the electron beam is parallel to $\langle 001 \rangle$, and the down-arrow symbol where it lies in the the plane of the platelet.

lying above the Raman frequency. The broadened black lines in Fig. 11(a) are indicative of an interaction between platelets in different unit cells. When the unit cells are constrained to the bulk lattice vectors, this interaction is greater than for the relaxed system. For the latter, the vibrational modes are strongly localized to the plane of interstitials. A further, more significant difference between the two plots is the locations of the modes lying above the Raman frequencies. For an unrelaxed cell dimension along z the highest modes at the zone center are around 13 cm^{-1} higher than when the cell is relaxed. Assuming that the cell relaxation of small platelets is less than that of larger ones (because of the constraining perfect lattice), this may account for the downward 20 cm^{-1} shift observed as platelets grow in size.

There is no evidence of deep gap states from the band structures of the platelet models, although it appears that there are strain induced states near the band edges. The absence of deep states is not unexpected given that all atoms are fully coordinated in an environment similar to that of bulk diamond.

There may, however, be changes to the nature of the states in the vicinity of the gap with consequent changes to the optical activity. Figure 12 shows the low-loss EEL spectra of the platelet along with that of bulk diamond, showing the effect of the platelet on the band-gap of the material. One can note characteristic differences to the spectrum caused by the platelet. In particular the trough around 11 eV is partially filled.

One also expects effects due to the polarization of the electron beam, and one can see from Fig. 12 this has little effect on the spectrum for the case of the relaxed volume. However, in contrast, the fixed volume case has a strong polarization effect, as indicated by the arrows in the figure, with the absorption perpendicular to the plane of the defect possessing the most significant departure from bulk absorption. In fact for this polarization the onset of absorption is deep into the band gap.

The implication of these results is that a shift of the conduction band near the platelet may affect the optical properties of nearby point defect: it is known that the N3 optical line, attributed to VN_3, is strongly affected by the presence of platelets.[49] However, the relatively high energy onset of the EEL spectrum in Fig. 12 means that something other than the perfect carbonaceous structure must be responsible for the low energy optical transitions.

C. Intraplatelet nitrogen

Platelets contain appreciable quantities of nitrogen and it is of interest to inquire into its properties. As a starting point we return to the I_4 building block. The energetically favored site for a single substitutional N atom in I_4 is where N replaces one of the carbon atoms in one of the four $\langle 001 \rangle$ split-interstitial sites. In the neutral charge state the N–C bond along $\langle 110 \rangle$ breaks, with the atoms moving apart so that the N atom becomes essentially planar with its three C neighbors.

Replacing one of the four atoms in every second I_4 unit by N leads to a nitrogen concentration of 12.5% of a monolayer defects for the platelet model shown in Fig. 8(b). This concentration is comparable with the lower limit observed.[12]

The binding energy of N with the platelet is given by

$$E^b(\text{N at platelet}) = E^f(\text{N}) + E^f(\text{platelet}) - E^f(\text{N at platelet}),$$

where $E^f(\text{N})$ is the formation energy per N atom and can be taken from any appropriate system, for example N_s, A, or B centers.

The single substitutional nitrogen atom is bound to the platelet by around 3 eV. It then follows from Sec. III A that the binding energy per nitrogen atom with respect to A and B centers is around 1 and 0 eV, respectively. In the case of the B defect, the formation energy includes the energy necessary to create a vacancy. This shows that platelets are competitive sinks for nitrogen along with B defects.

Figure 13 shows the electronic structure of a single nitrogen atom in the platelet. In this diagram the electronic structures have been aligned using the average potentials for each system. A half-filled level lies around mid-gap and which is localized partly on the N atom, but predominantly on a carbon neighbor in a similar way to the isolated substitutional nitrogen defect.[19] Mid-gap optical transitions, around 2–3 eV, to the band edges would then be expected.

A single N defect attached to the platelet as described above is not the most stable defect. Replacing a pair of neighboring $\langle 001 \rangle$ aligned C atoms in each I_4 by nitrogen leads (Fig. 14) to a more stable defect. Each N atom is threefold coordinated but all C atoms remain four-fold coordinated. The binding energy of this defect relative to two isolated N impurities *within the platelet* is 2.2 eV. With respect to nitrogen taken from N_s, A, or B centers in the bulk, the binding energies are 7.7, 3.7, and 1.1 eV, respectively. N concentrations up to 25% of a monolayer can arise by the

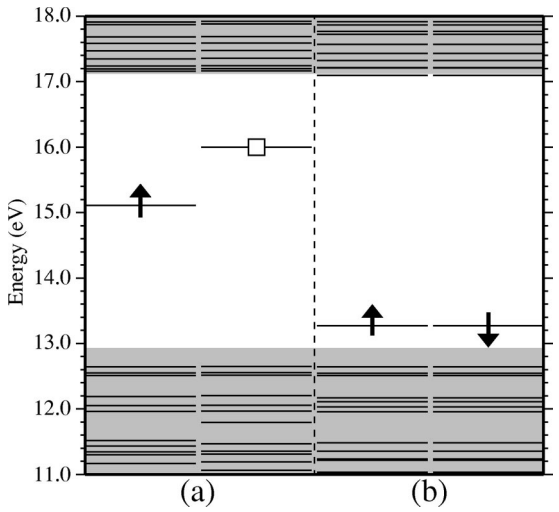

FIG. 13. Spin-polarized Kohn-Sham levels at the zone center for (a) the single and (b) the dinitrogen defects within the platelet model shown in Fig. 8(b). In each case the left hand set are the spin-up spectra and the right hand set spin-down. The shaded regions show the locations of the band edges of bulk diamond. The arrows indicate the filled gap levels and white square shows the empty gap level.

replication of the defect among I_4 units in the platelet. This form of nitrogen is then more stable than *B* centers.

The Kohn-Sham energy levels of the platelet containing one of these nitrogen dimers consists of a filled level in the gap close to the valence band top (Fig. 13). An optical transition could occur between this state and the conduction band edge, leading to a high energy (>4 eV) transition. Such transitions could lead a broad optical band consistent with observations when the interactions between different dimers are considered. Polarization effects observed for the 990- and 491-nm absorption bands could be explained as arising from the nitrogen related levels whose wavefuntions are localized to the platelet.

Finally, we consider the Lang model of Fig. 1, where each I_4 unit is replaced by four N atoms. The lattice displacement

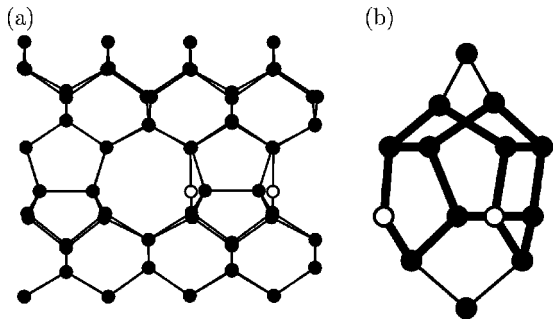

FIG. 14. (a) Projection of the platelet containing a pair of nitrogen atoms, indicated by the white circles. Compare with Fig. 10. (b) shows a view of the structure so that the I_4 building block can be seen more clearly. The thicker bonds indicate the five-member rings characteristic of the platelet models. The nitrogen dimer leads to the breaking of one reconstructed bond of the purely carbonaceous model.

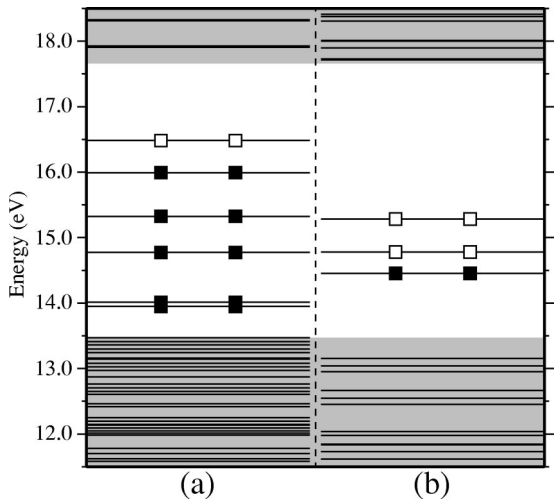

FIG. 15. Kohn-Sham levels at the Brillouin-zone center of the vacancy in the platelet when (a) the $\langle 001 \rangle$ cell length is constrained and (b) relaxed for the platelet shown in Fig. 8(b). The shaded area shows the locations of the band edges in bulk diamond. Filled squares indicate occupied gap levels and white squares show empty gap levels.

associated with this platelet is calculated to be only $\sim 0.3a_0$ and smaller than the lowest measured value for the platelets.[10] This supports Humble's original objection to the Lang model described above in Sec. I. The formation energy per N atom for the Lang model is about 0.5 eV higher than that of the *B* center and hence the model is also ruled out on energetic grounds.

In summary, although a purely carbonaceous model is not stable in the presence of sufficient mobile nitrogen, complete replacement of self-interstitials by nitrogen is energetically unfavorable. It seems then that the variation in the nitrogen concentration in platelets is due to a mixture of nitrogen solubility and kinetic factors. Hence type Ia diamonds subjected to high temperatures for sufficiently long will possess platelets containing greater concentrations of nitrogen. This is one way in which "'manmade'' platelets will differ from natural ones.

D. Vacant sites

Since the platelet is built of carbon interstitials, an obvious defect is a vacant site. Such a defect is similar to a vacancy in bulk diamond although the tetrahedral symmetry is lifted through the presence of the platelet. In the simulations where the volume of the cell is fixed, there is some reconstruction which yields only two dangling bonds, but two of the vacancy neighbors possess bond lengths and angles far from those of bulk diamond. This can be viewed as a defect akin to the $O3$ center, illustrated in Fig. 2(a). In the volume relaxed case there is no reconstruction, producing a defect with four carbon sites with three bonds. In either case, the dangling bonds associated with the vacancy give rise to a number of gap levels, some of which are empty, as shown in Fig. 15 for the cases where the $\langle 001 \rangle$ dimension of the unit cell has been (a) fixed land (b) relaxed. In Fig. 15(a), several filled states are pushed into the gap (above the bulk

valence-band top shown by the lower shaded area) due to the internal strains which lead to the narrowing of the band-gap, and are not related directly to the vacancy. Figure 15 clearly shows the effect of relaxation is considerable and thus the precise location of filled and empty levels is sensitive to the local strain. Different vacant sites in the platelet would then be expected to lead to broadened optical transitions. This might be the origin of the 1.25-eV platelet absorption band. The formation energy of a vacant site is about 4.5 eV and about 1.5–2.5 eV lower than the formation energy of a vacancy in the bulk. Thus a vacancy is bound to the platelet by this amount. It is highly likely that nitrogen would bind at neighboring sites and such centers would be further sources of optical transitions, particularly at low energy.

E. Non {001}-oriented platelets

1. {*113*} *defects*

The RLDs shown in Fig. 6 were investigated using a face-centered-cubic cell made from $6\times6\times1$ primitive cells, each containing two carbon atoms. We first investigate the structure of a chain of interstitials lying along $\langle 1\bar{1}0\rangle$ as shown in Fig. 5. The energies per interstitial of the three structures given in Figs. 5(a), 5(b) and 5(c) are respectively 4.6, 3.4, and 3.5 eV. This shows that the bond switching results in a release of strain energy. The 0.1 eV difference in (b) and (c) is probably not significant, and the ratio of the formation energies of (a):(c) is close to that found previously for silicon.[41] The energies approximately scale with the cohesive energies of silicon and diamond.

We now investigate the effect of packing chains in a {113} plane as shown in Figs. 6(a)–6(c). These structures differ in the separation of the chains along $\langle\bar{3}\bar{3}2\rangle$. We constructed several unit cells containing between 44 and 132 atoms with two to eight interstitials per cell and whose neighboring cells represent a periodic continuation of the platelet along $\langle\bar{3}\bar{3}2\rangle$ and $\langle 1\bar{1}0\rangle$. The energies of these models are 1.7, 1.9 and 1.4 eV respectively. It is important to allow the unit cell to relax along $\langle 113\rangle$ as this has a large effect on the resulting formation energy.[32] Our conclusion is that these structures have a higher energy than the {001} platelet in Fig. 8(b) whose formation energy per interstitial is only 0.9 eV. This is consistent with the view that RLDs do not form in diamond.

2. {*111*}*-planar defects*

The structure shown in Fig. 7 was embedded in a $\langle 111\rangle$ oriented unit cell containing 36 atoms plus two self-interstitials. The resulting formation energy per interstitial is 2.9 eV per interstitial which drops to around 1.6 eV when the $\langle 111\rangle$ lattice parameter is allowed to relax. The $\langle 111\rangle$ dilation is approximately $3\langle 111\rangle a_0/20$. The formation energy is similar to the {113} RLDs, and around 60% higher than those of the {001} platelet models, confirming the stability of the {001} platelet models discussed in Sec. III B.

IV. DISCUSSION AND CONCLUSIONS

Following earlier publications of preliminary results on the platelets in diamond,[29,30] we have confirmed and extended the theoretical understanding of the Humble structures platelets in diamond. As found previously, our preferred model based on carbon interstitials is consistent with TEM and optical studies. The lowest energy carbon interstitial platelet, shown in Fig. 8(b), has a lattice displacement in agreement with observations and the inequivalence of the $\langle 110\rangle$ and $\langle 1\bar{1}0\rangle$ projections is consistent with TEM. However, the closeness of the energies for models (a), (c), (d), and (e) in Fig. 8 suggests that disordered platelets containing several of these models are possible. All the models give local vibrational modes lying above the bulk Raman frequency and close to the B' band assigned to platelets. By examination of the Kohn-Sham spectrum and by calculating the electron energy loss spectrum for the platelet structure, we have shown in this study that the platelet does not possess deep electronic gap levels. However, the strain associated with small platelets possibly leads to shallow empty levels. These might promote optical transitions from point defects close to the platelet. Nitrogen and vacant sites are candidates for these. The former is strongly bound to the platelet as a pair. We have also found that the Lang model containing two monolayers of nitrogen is less stable than a collection of *B* centers dissolved in the lattice and furthermore possesses a displacement vector of just $0.3a_0$, at variance with experiment.

We have now shown that the transformation of substitutional nitrogen atoms into close-pair defects (*A* centers), and VN_4 defects (*B* centers) is exothermic even when a vacancy is created in the latter case. However, the calculations show that rate of formation of *B*-centers along with self-interstitials is too slow to explain the formation of {001} platelets, and inconsistent with experimental data. This conflicts with the original proposal of Woods[15] that interstitials released by *B* centers formed platelets. Rather, we present in this paper the argument that the finite platelet is to be regarded as a partial dislocation with Burgers vector $\langle 00R\rangle$ with $R\sim0.4a_0$, and it is the *climb* of this partial which leads to platelet growth by the release of vacancies which are subsequently trapped at *A* centers resulting in relatively mobile VN_2 defects ($H3$ defects). There are then trapped by *A* centers to give immobile *B* centers (VN_4). The activation energy for this process is estimated to be about 8 eV, in reasonable agreement with experimental data for the growth of *B* centers and platelets. The whole process is exothermic as the binding energy of an interstitial with a large platelet is about 11 eV, while the cost in forming a *B* center together with an isolated interstitial is 8.3 eV. Of course, this raises a question about the nucleation of the platelets. A Burgers vector analysis shows that platelets are more stable than *small* $\langle 110\rangle$ perfect dislocation loops and thus the nuclei for the platelet might be pre-existing I_4 defects. However, the energy per unit area of the platelet suggests a stable radius of only a few nano-meters and much smaller than the sizes observed. This implies that the platelets are metastable and would shrink in the presence of excess vacancies or transform to lower energy perfect loops by interaction with glide dislocations as has been discussed.[26]

There is an essential difference with the growth of interstitial extended defects in silicon arising either from implan-

tation or oxygen precipitation. The formation energies of vacancies and interstitials in Si are believed to be roughly equal ($\sim 3-4$ eV) quite unlike diamond where the self-interstitial possesses formation energy twice that of the vacancy, and is very large (~ 12 eV). Consequently, reactions requiring isolated interstitials, e.g., some types of impurity diffusion, are less likely to occur in diamond than in silicon.

Finally, we have shown that {001} interstitial platelets in diamond are unlike the planar interstitial aggregates seen in silicon: the rodlike defects observed there consisting of $\langle 110 \rangle$ chains of interstitials have a relatively high energy in diamond, probably because of the difficulty of inserting chains into small $\langle 110 \rangle$ channels.

ACKNOWLEDGMENTS

We thank T. Evans, I. Kiflawi, M. I. Heggie, and A. R. Lang for informative discussions. P. B. Hirsch is especially thanked for a clarification of the mechanisms of platelet degradation.

[1] G. S. Woods, Philos. Mag. **34**, 993 (1976).
[2] I. Kiflawi and A. R. Lang, Nature (London) **267**, 36 (1977).
[3] C. V. Raman and P. Nilakantan, Proc.-Indian Acad. Sci., Sect. A **11**, 389 (1940).
[4] F. C. Frank, Proc. R. Soc. London, Ser. A **237**, 168 (1956).
[5] T. Evans and C. Phaal, Proc. R. Soc. London, Ser. A **270**, 538 (1962).
[6] W. Kaiser and W. L. Bond, Phys. Rev. **115**, 857 (1959).
[7] A. R. Lang, Proc. Phys. Soc. London **84**, 871 (1964).
[8] J. C. Barry, L. A. Bursill, and J. L. Hutchison, Philos. Mag. A **51**, 15 (1985).
[9] P. Humble, J. K. KacKenzie, and A. Olsen, Philos. Mag. A **52**, 605 (1985).
[10] D. Cherns, K. Kaneko, A. Hovsepian, and A. Lang, Philos. Mag. A **75**, 1553 (1997).
[11] S. D. Berger and S. J. Pennycook, Nature (London) **298**, 635 (1982).
[12] P. J. Fallon, L. M. Brown, J. C. Barry, and J. Bruley, Philos. Mag. A **72**, 21 (1995).
[13] J. Bruley, Philos. Mag. Lett. **66**, 47 (1992).
[14] I. Kiflawi, J. Bruley, W. Luyten, and G. Van Tendeloo, Philos. Mag. B **78**, 299 (1998).
[15] G. S. Woods, Proc. R. Soc. London, Ser. A **407**, 219 (1986).
[16] E. V. Sobolev, V. E. Il'in, S. V. Lenskaya, and O. P. Yur'eva, J. Appl. Spectrosc. **9**, 1108 (1968).
[17] G. Davies, J. Phys. C **9**, L537 (1976).
[18] J. H. N. Loubser and J. A. van Wyk (unpublished).
[19] R. Jones, P. R. Briddon, and S. Öberg, Philos. Mag. Lett. **66**, 67 (1992).
[20] P. R. Briddon, R. Jones, and M. I. Heggie, in *Proceedings of the International Conference on New Diamond Science and Technology*, edited by R. Messier, J. T. Glass, J. E. Butler, and R. Roy (Materials Research Society, Pittsburgh, 1991), p. 63.
[21] T. Evans and Z. Qi, Proc. R. Soc. London, Ser. A **381**, 159 (1982).
[22] G. S. Woods, I. Kiflawi, H. Kanda, and T. Evans, Philos. Mag. B **67**, 651 (1993).
[23] S. G. Clackson, M. Moore, J. C. Walmsley, and G. S. Woods, Philos. Mag. B **62**, 115 (1990).
[24] B. P. Allen and T. Evans, Proc. R. Soc. London, Ser. A **375**, 93 (1981).
[25] T. Evans, I. Kiflawi, W. Luyten, G. van Tendeloo, and G. S. Woods, Proc. R. Soc. London, Ser. A **449**, 295 (1959).
[26] P. B. Hirsch, P. Pirouz, and J. C. Barry, Proc. R. Soc. London, Ser. A **407**, 239 (1986).
[27] P. Humble, Proc. R. Soc. London, Ser. A **381**, 65 (1982).
[28] B. J. Coomer, J. P. Goss, R. Jones, S. Öberg, and P. R. Briddon, J. Phys.: Condens. Matter **13**, L1 (2001).
[29] J. P. Goss, B. J. Coomer, R. Jones, C. J. Fall, C. D. Latham, P. R. Briddon, and S. Öberg, J. Phys.: Condens. Matter **12**, 10257 (2000).
[30] J. P. Goss, B. J. Coomer, R. Jones, T. D. Shaw, P. R. Briddon, M. Rayson, and S. Öberg, Phys. Rev. B **63**, 195208 (2001).
[31] G. S. Woods, Philos. Mag. Lett. **59**, 339 (1989).
[32] J. P. Goss, R. Jones, and P. R. Briddon, Phys. Rev. B **65**, 035203 (2002).
[33] D. C. Hunt, D. J. Twitchen, M. E. Newton, J. M. Baker, T. R. Anthony, W. F. Banholzer, and S. S. Vagarali, Phys. Rev. B **61**, 3863 (2000).
[34] D. J. Twitchen, M. E. Newton, J. M. Baker, O. D. Tucker, T. R. Anthony, and W. F. Banholzer, Phys. Rev. B **54**, 6988 (1996).
[35] D. J. Twitchen, M. E. Newton, J. M. Baker, T. R. Anthony, and W. F. Banholzer, J. Phys.: Condens. Matter **13**, 2045 (2001).
[36] J. M. Baker, Diamond Relat. Mater. **7**, 1282 (1998).
[37] D. C. Hunt, D. J. Twitchen, M. E. Newton, J. M. Baker, J. K. Kirui, J. A. van Wyk, T. R. Anthony, and W. F. Banholzer, Phys. Rev. B **62**, 6587 (2000).
[38] R. Jones, J. Coutinho, S. Öberg, and P. R. Briddon, Physica B **308-310**, 8 (2001).
[39] J. L. Mercer, J. S. Nelson, A. F. Wright, and E. B. Stechel, Model. Simul. Mater. Sci. Eng. **6**, 1 (1998).
[40] M. Kaukonen, R. Jones, S. Öberg, and P. R. Briddon, Phys. Rev. B **64**, 245213 (2001).
[41] J. Kim, J. W. Wilkins, F. S. Khan, and A. Canning, Phys. Rev. B **55**, 16 186 (1997).
[42] T. A. G. Eberlein, N. Pinho, R. Jones, B. J. Coomer, J. P. Goss, P. R. Briddon, and S. Öberg, Physica B **308-310**, 454 (2001).
[43] R. Q. Hood, P. R. C. Kent, R. J. Needs, and P. R. Briddon (unpublished).
[44] T. Evans, Z. Qi, and J. Maguire, J. Phys. C **14**, 379 (1981).
[45] D. R. Wright, P. J. Dean, E. C. Lightowlers, and C. D. Mobsby, J. Lumin. **4**, 169 (1971).
[46] S. Desgreniers, Y. K. Vohra, and A. L. Ruoff, Solid State Commun. **70**, 705 (1989).
[47] N. Sumida and A. R. Lang, Proc. R. Soc. London, Ser. A **419**, 235 (1988).
[48] A. T. Collins and G. S. Woods, Philos. Mag. B **45**, 385 (1982).
[49] A. P. Yelisseyev and E. V. Sobolev, Superhard Mater. **1**, 19 (1979).
[50] R. Brydson, L. M. Brown, and J. Bruley, J. Microsc. **189**, 137 (1998).

[51] S. Muto and S. Takeda, Philos. Mag. Lett. **72**, 99 (1995).
[52] S. Takeda, in *Proceeding of the 10th Conference on Microscopy of Semiconducting Materials*, edited by A. G. Cullis and J. L. Hutchison, IOP Proc. No. 157 (Institute at Physics and Physical Series, Bristol, 1997), p. 25.
[53] S. Takeda, Jpn. J. Appl. Phys. **30**, L639 (1991).
[54] M. Kohyama and S. Takeda, Phys. Rev. B **46**, 12 305 (1992).
[55] S. Takeda, M. Kohyama, and K. Ibe, Philos. Mag. A **70**, 287 (1994).
[56] S. Takeda and T. Kamino, Phys. Rev. B **51**, 2148 (1995).
[57] J. Kim, F. Kirchhoff, J. W. Wilkins, and F. S. Khan, Phys. Rev. Lett. **84**, 503 (2000).
[58] L. Fedina, A. Gutakovskii, A. Aseev, J. Van Landuyt, and J. Vanhellemont, Philos. Mag. A **66**, 423 (1998).
[59] L. Fedina, A. Gutakovskii, A. Aseev, J. Van Landuyt, and J. Vanhellemont, Phys. Status Solidi A **171**, 147 (1999).
[60] C. T. Chou, D. J. H. Cockayne, J. Zou, P. Kringhøj, and C. Jagadish, Phys. Rev. B **52**, 17 223 (1995).
[61] C. A. Ferreira-Lima, Ph.D. thesis, University of Cambridge, U.K., 1975.
[62] J. Coutinho, R. Jones, P. R. Briddon, and S. Öberg, Phys. Rev. B **62**, 10 824 (2000).
[63] R. Jones and P. R. Briddon, in *Identification of Defects in Semiconductors*, *Semiconductors and Semimetals*, Vol. 51A, edited by M. Stavola (Academic, Boston, 1998), Chap. 6.
[64] H. J. Monkhorst and J. D. Pack, Phys. Rev. B **13**, 5188 (1976).
[65] G. B. Bachelet, D. R. Hamann, and M. Schlüter, Phys. Rev. B **26**, 4199 (1982).
[66] D. A. Liberman, Phys. Rev. B **62**, 6851 (2000).
[67] J. E. Northrup, R. Di Felice, and J. Neugebauer, Phys. Rev. B **56**, R4325 (1997).
[68] M. J. P. Musgrave and J. A. Pople, Proc. R. Soc. London, Ser. A **268**, 474 (1962).
[69] C. J. Fall, R. Jones, P. R. Briddon, A. T. Blumenau, T. Frauenheim, and M. I. Heggie, Phys. Rev. B **65**, 245304 (2002).
[70] C. J. Fall, A. T. Blumenau, R. Jones, P. R. Briddon, T. Frauenheim, A. Gutiérrez-Sosa, U. Bangert, A. E. Mora, J. W. Steeds, and J. E. Butler, Phys. Rev. B **65**, 205206 (2002).
[71] T. Miyazaki, H. Okushi, and T. Uda, Phys. Rev. Lett. **88**, 066402 (2002).
[72] J. P. Goss, R. Jones, M. I. Heggie, C. P. Ewels, P. R. Briddon, and S. Öberg, Phys. Rev. B **65**, 115207 (2002).
[73] A. Mainwood, Phys. Rev. B **49**, 7934 (1994).
[74] S. J. Breuer and P. R. Briddon, Phys. Rev. B **51**, 6984 (1995).
[75] G. Davies, S. C. Lawson, A. T. Collins, A. Mainwood, and S. J. Sharp, Phys. Rev. B **46**, 13 157 (1992).
[76] L. Allers, A. T. Collins, and J. Hiscock, Diamond Relat. Mater. **7**, 228 (1998).
[77] S. Takeuchi and K. Suzuki, Phys. Status Solidi A **171**, 99 (1999).
[78] P. Humble, D. F. Lynch, and A. Olsen, Philos. Mag. A **52**, 623 (1985).
[79] J. C. Barry, Philos. Mag. A **64**, 111 (1991).
[80] J. P. Hirth and J. Lothe, *Theory of Dislocations*, *Materials Science and Engineering* (McGraw-Hill, New York, 1968).
[81] Note, the displacements quoted in the previous, preliminary publications (Refs. 29 and 30) differ from those in Table II because they were determined from the local dilation of the {001} planes immediately above and below the platelet, rather than from the changes in the unit cell geometry as described Sec. III B 2.